Mechanical characterisation of single cellulosic fibres

Julia Auernhammer, Robert W. Stark,
Technical University of Darmstadt, Institute of Materials Science, Physics of Surfaces

INTRODUCTION:

An excellent tool to study and characterise the physical properties of solid samples is the atomic force microscope (AFM). The AFM is not only useful for imaging the topography, but also to quantify the mechanical properties. One operation mode of the AFM is the quasi-static "PeakForce-Tapping mode"(B. Pittenger 2012), which provides access to mechanical properties such as elastic modulus, adhesion, dissipation and deformation of the sample at the nanoscale. Furthermore, from mapping with static force vs. distance curves it is possible to reconstruct the topography or mechanical properties such as the Young's modulus and the maximum indentation depth into the sample. Thus, a three-dimensional nanomechanical characterisation can be obtained. AFM measurements are not only limited to the use in dry conditions, also measurements in liquid can be accomplished at high resolution.

Paper, as a high-tech material made from cellulose, has promising applications in areas such as electronics, sensor technology, microfluidics and medicine (Bump et al. 2015; Delaney et al. 2011; Gurnagul and Page 1989; Hayes and Feenstra 2003; Liana et al. 2012; Ruettiger et al. 2016). Cellulose is a natural material, is abundant and renewable, and is the most important raw material in the papermaking industry. But, the use of paper as substrate material in technical applications is raising some challenges. For example, the production from natural fibres or the loss of the mechanical stability of fibres in wet state.

As cellulose has a hygroscopic character and is insoluble in water, the fibres begin to swell, become more flexible and thus, the strength of the paper sheet is decreasing (Cabrera et al. 2011; Dunlop-Jones 1996; Fidale et al. 2008; Gumuskaya et al. 2003; Janko et al. 2015; John and Thomas 2008; Lindman et al. 2010; Rogovin and Gal'brajch 1983). Hence, the understanding of the loss of mechanical properties in wet state has to be tackled. As paper is consisting of single fibres, the knowledge of the loss of mechanical stability has to be built from bottom up. Therefore, this work is focussing on single fibres and their mechanical behaviour at dry state and increasing relative humidity (RH).

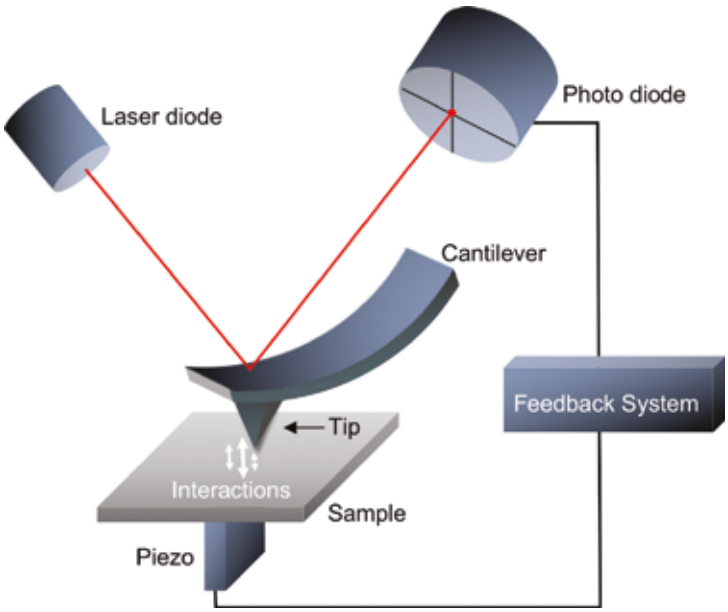

Furthermore, the challenge to improve the wet-strength has to be tackled. So far, Polyamidoarminepichlorohydrin (PAAE) resins are the most commonly used wet strength agents (H. Pahl 1988; Yano et al. 1991). In addition to all the advantages of increasing strength in dry and wet conditions, PAAE resins in particular have some disadvantages e.g. reusability is greatly reduced, or halogen by-products can cause environmental pollution. Thus, alternative polymers have to be investigated to increase the wet-strength of paper.

1. The Atomic Force Microscope (AFM)

The atomic force microscope (AFM) was firstly presented in 1968 by Binning, G. et al. [67]. It belongs to the category of the scanning probe microscopes (SPM). In general, a SPM consist of a sharp tip that scans the sample line by line while the interactions between the surface and the tip are detected and a feedback system that controls the scanning process.

The set-up of an atomic force microscope in figure 1 shows a laser diode, a sample, a cantilever with a sharp tip, a four-segmented photodiode, a feedback system, and a piezo element for an x-, y-, z-movement of the sample and the cantilever. The working principle behind the AFM is to detect the interactions between the tip and the surface atoms of the sample. For this purpose, the laser beam is focused on the reflectively coated back of the cantilever, which is directed onto the four-segmented photodiode. In the rest position, the laser beam hits the centre of the photodiode, which induces the same proportion of current in each segment due to the photoelectric effect. When interactions between tip and surface are detected, the cantilever bends and the laser beam changes its position on the photodiode. Therefore, a different proportion of current is now induced in each segment. The difference in the induced current is detected. The difference between the upper and lower segment is an indicator of the vertical bending of the cantilever and is used to record the topography. The difference between left and right is described as an indicator of the lateral forces acting on the tip. The evaluated signal from the photodiode is processed further in the feedback system.

Figure 1: Schematic set up of an Atomic Force Microscope (AFM).

2. Mechanical properties in AFM measurements

In AFM measurements it is possible to record mechanical properties in operation modes, where the tip touches the sample surface. In these operation modes force vs. distance curves are generated at every measuring point on the sample surface. Via recording force-distance curves it is possible to detect mechanical properties of surfaces.

In figure 2, the blue line represents the characteristics during the approach of the tip towards the surface and the red line that during the retraction of the tip. When the tip approaches the surface, a "snap-into-contact" point occurs at a certain distance near the surface (d0). Here the attractive force gradient is greater than the spring constant of the cantilever and the tip snaps into the surface. Then the set PeakForce is applied to the surface, which results in a deformation of the sample. When the PeakForce setpoint has been reached, the tip is pulled back from the surface. An adhesive force now occurs between the tip and the surface. Further mechanical properties of the surface can be read from this curve. The elastic properties can be described by contact models such as Hertz model, Derjaguin-Muller-Toporov (DMT) model, or Johnson-Kendall-Roberts (JKR) model (Derjaguin et al. 1975b; Hertz 1881; Johnson et al. 1971). The respective modulus is fitted within the green line in figure 2. The dissipation can be calculated from the integrated area between approach and withdraw curve.

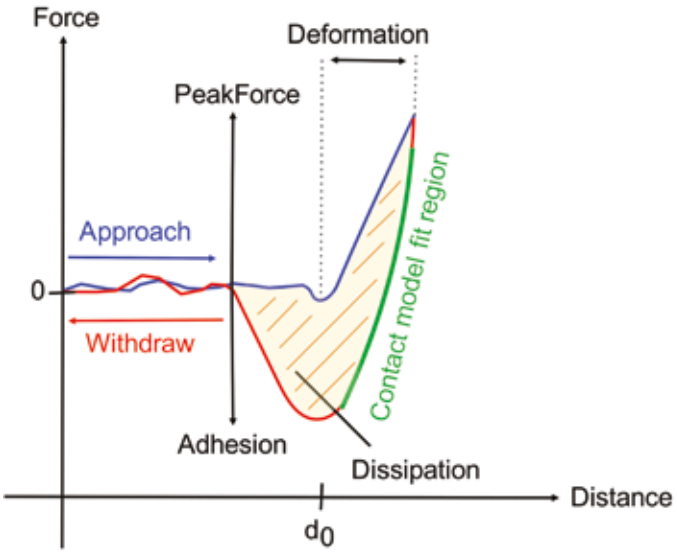

Figure 2: Schematics of a force-distance curve with the mechanical properties which can be determined.

2.1 Recording static force-distance curves

Scanning bending test

One method to determine mechanical properties of single cellulosic fibres is to record static force-distance curves along the fibre axis. This method can be called as "scanning bending test". In the scanning bending test, the sharp tip is exchanged with a colloidal probe to provide a defined contact area. It is schematically shown in figure 3a). This method allows to detect the mechanical properties on every local spot on a single fibre. Furthermore, the scanning bending test circumvents the problem of assuming homogenised fibre dimensions as in the common bending test, which is usually performed in the centre of the fibre only. Additionally, the local variations within the fibre diameters can be included in the scanning bending test. The local fibre diameter in every bending point of the fibre can be analysed via confocal laser scanning microscopy (CLSM). With the scanning bending test, it is possible to detect mechanical properties from the force-distance curves such as adhesion or dissipation, but it is also possible to calculate the contact stress and the strain. Therefore, a whole mechanical image of a fibre along its longitudinal axis can be displayed (Auernhammer et al. 2021b).

In figure 3b) a schematic force-bending curve is shown. The transformation between force-distance curve to a force-bending curve is necessary to extract the bending ability of the local fibre spot. Here, the contact point of the probe and sample is detected and set to zero. Then, the bending distance can be read out. Furthermore, it is possible to extract several bending abilities for different forces to detect a potentially nonlinear local response of the fibre as schematically shown in figure 3b). The resulting contact area of a colloidal probe and a curved cylinder (fibre) is elliptical shaped as shown in figure 3c).

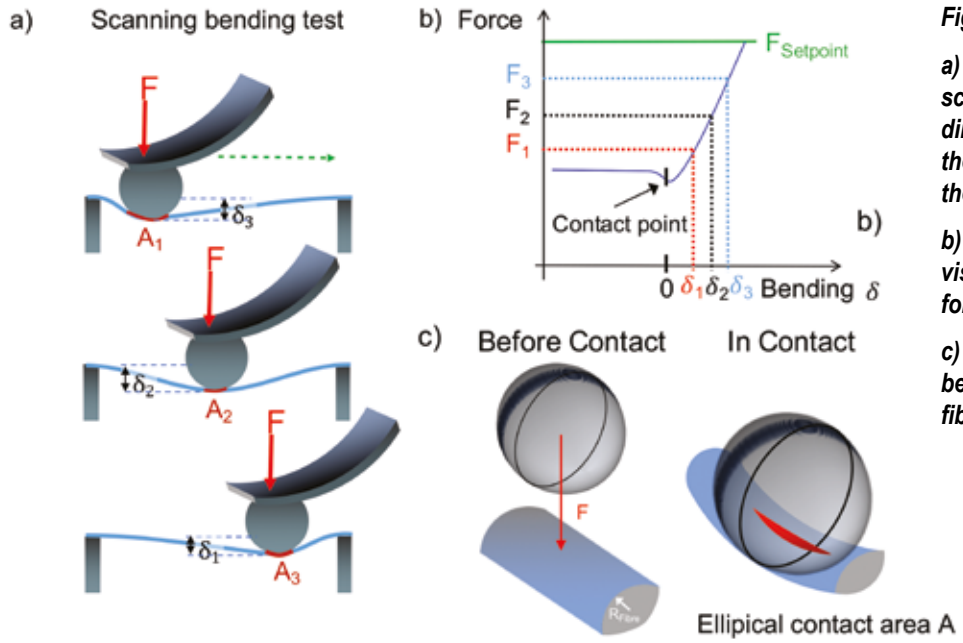

Figure 3:

a) Schematics of the section-wise scanning process along the longitudinal direction of the fibre. At every section, the scanning trajectory was realigned to the fibre axis.

b) Force-bending curve with visualization of multiple virtual setpoint forces F.

c) Schematics of the contact mechanics between the colloidal probe and the fibre before contact and in contact.

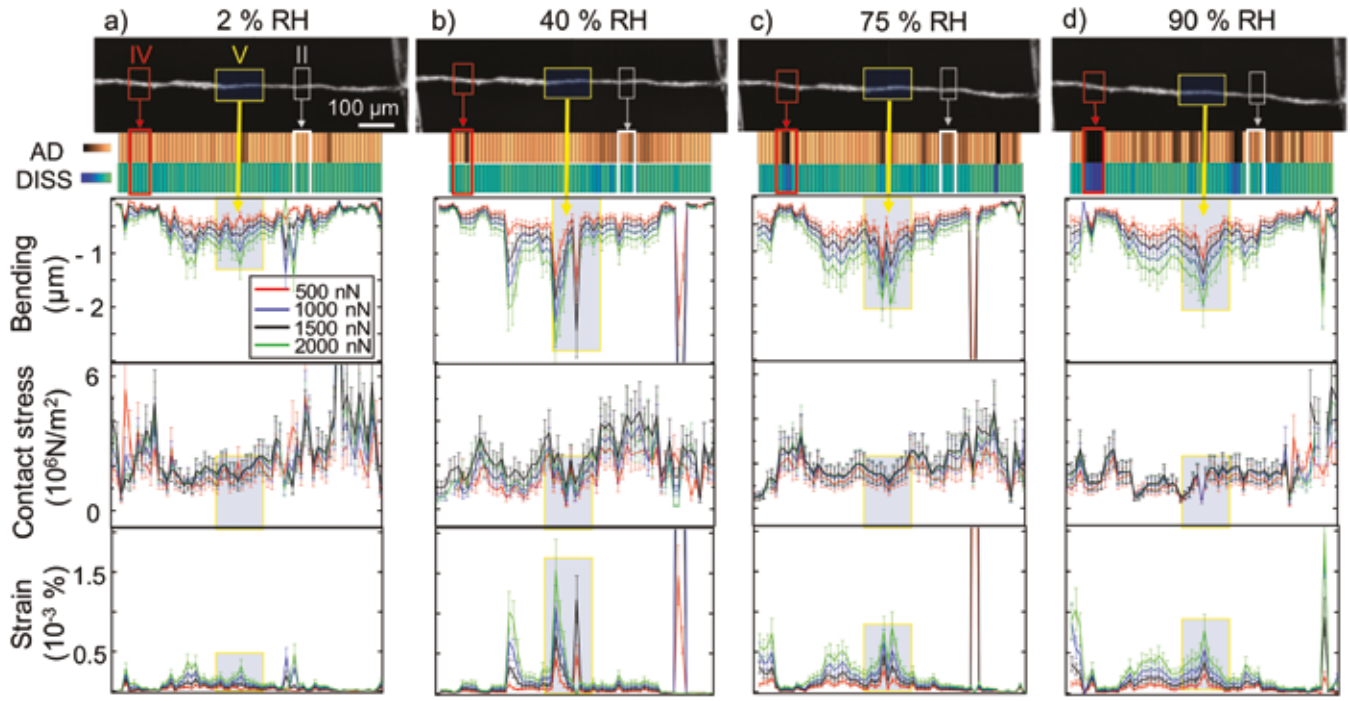

Figure 4: Mechanical characterisation of a cellulose fibre along its longitudinal direction.

From top to bottom: CSLM image of the fibre with the local adhesion and dissipation maps along the fibre beneath. The scale bars are -800 to 0 nN (adhesion) and 1 to 1 x105 J (dissipation).

Beneath: bending behaviour, contact stress (error 30 %) and strain (error 25 %) along the fibre.

The mechanical properties in a) are at 2 % RH, b) at 40 % RH, c) 75 % RH and d) 90 % RH (Auernhammer et al. 2021b).

In figure 4, results of the scanning bending tests are shown. To detect the local changes in the mechanical properties with increasing RH, it was increased stepwise from 2 %, to 40 %, to 75 % and to 90 % RH.

Figure 4 shows at each RH the CLSM image of the fibre, beneath the local adhesion map, the dissipation map, the corresponding bending ability and the calculated contact stress and strain. From the recording of the local mechanical properties via the scanning bending test, it can be shown that the adhesion and the dissipation increase with increasing RH. From the bending data in figure 4, the local bending increased when increasing the RH from 2 % RH to 90 %. Additionally, mechanical effects (clamping) play a role: the bending of the fibre is reduced at both fixed ends and is increased in the middle of the fibre. Here, the reduced bending at both ends is due to attachment to the sample holder. Additionally, “soft spots” could be identified at an intermediate RH of 40 %. Increasing the RH, the soft areas became less distinctive when the entire fibre became softer. This implies that at intermediate RH, individual soft spots can occur in a cotton linter fibre weakening the fibre locally, whereas the entire fibre softens at elevated RH. In the contact stress graphs in figure 4, it is evident that the contact stress was higher at both ends of the fibre. This is due to the attachment at the fixed ends and should not be interpreted as a higher strength of the fibre. The contact stress at both fixed ends decreases as the RH is increased. Additionally, here, the increased amount of water molecules inside the cellulose network destroys bonds and act as a lubricant between the fibrils, which leads to fibre softening. The strain is linked to the bending properties of the fibre. Thus, the strain behaviour follows the same trend as the bending behaviour and is assumed to be interpreted identically.

With the scanning bending test, it is possible to measure mechanical properties of a free hanging fibre (clamped at both ends) with colloidal probe atomic force microscopy along the longitudinal direction of the fibre. The proposed method of scanning along the longitudinal direction of the fibre provides a more detailed picture of the mechanical behaviour. To demonstrate the potential of this approach, the mechanical properties of a single cellulose fibre were mapped for varying RH. This method can be applied for different fibre types, plain fibres or coated fibres to test, analyse and detect differences in their mechanical behaviour.

2.2 Recording quasi-static force-distance curves

PeakForce-Tapping mode

One other method to record mechanical properties of single cellulosic fibres is the mapping of the local mechanical properties via quasi static force-distance curves in a small area of the fibre. This method is described as “PeakForce-Tapping” (B. Pittenger 2012). Here, the sharp tip attached to the cantilever is oscillated below resonance and is moved (scanning motion) over the fibre surface. The quasi-static PeakForce-Tapping mode allows for the simultaneous mapping of the topography and mechanical properties. Here, cumulative force vs. distance curves were measured at every pixel in the recorded map. The mechanical properties were then directly extracted from the force-distance curves (see figure 2). While the adhesion force represents the minimum in the retract curve, the DMT modulus was fitted with the prediction of the contact mechanics by Derjaguin, Muller, and Toporov (DMT) (Derjaguin et al. 1975a).

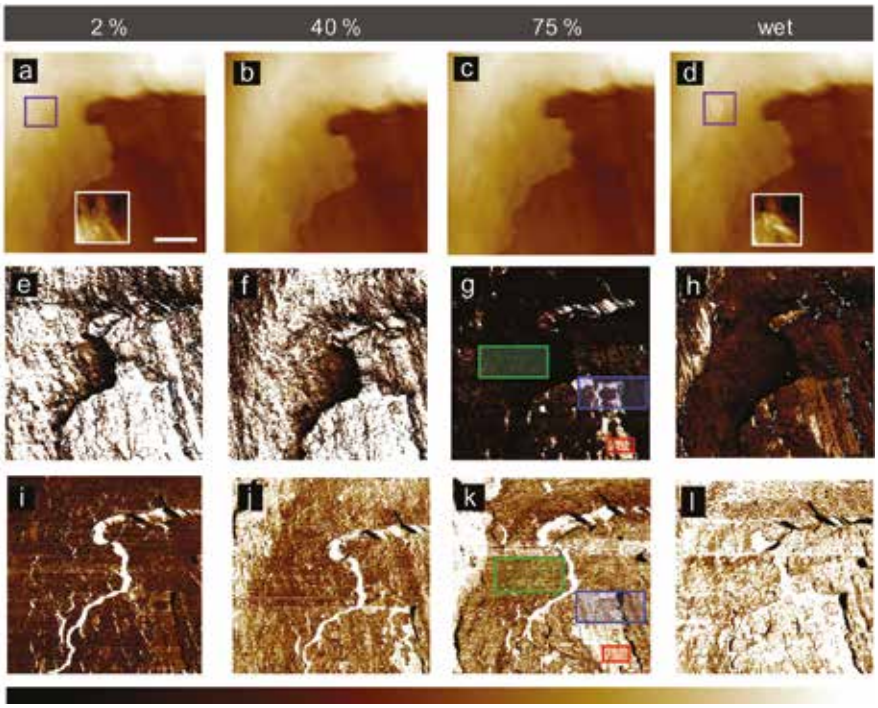

Figure 5:

AFM images of plain fibres. The RH was varied from 2 % to a wet condition. (a-d) Topography images, (e-h) DMT modulus maps and (i-l) adhesion maps. The scale bar is 800 nm.

The colour bar is -1 – 1.3 µm for topography images, 0 – 3 GPa for DMT modulus maps and 0 – 2 nN for adhesion maps.

In the white framed topography images, the colour scale was modified to 0 – 250 nm.

The white boxed images in a) and d) show the topography of the swollen microfibrils.

An amorphous region of cellulose is highlighted in green, while the crystalline region is marked in red, and a transition between crystalline and amorphous regions is shown in blue.

(Auernhammer et al. 2021a)

In figure 5, the topography as well as the mechanical properties of the plain fibres as a function of the RH are shown (Auernhammer et al. 2021a). As shown in figure 5, the plain fibre exhibited crystalline and amorphous regions in the topography image, but especially in the mechanical property maps, such as the DMT modulus and adhesion, the differences in the crystal structure of cellulose were clearly distinguishable. In the mechanical property maps, the adhesion increased with increasing RH, while the DMT modulus decreased. Overall, swelling of microfibrils was observed in the AFM topography images as the RH was increased. Figure 5a shows the topography image with the microfibrils at 2 % RH. Comparing the microfibrils in figure 5a to those in figure 5d, which shows a fully hydrated fibre, the microfibrils appear to be swollen under wet conditions. The white box (figure 5a, d) indicates in detail the swelling of microfibrils due to absorbed water inside the cellulose network. The insolubility of cellulose results in swelling of the microfibrils (Lindman et al. 2010). Water infiltrates the network and diffuses through the pore space system by capillary condensation. Therefore, the volume increases, which leads to an expansion in the crystal structure and eventually breaks the hydrogen bonds in the cellulose network (Cabrera et al. 2011; Gumuskaya et al. 2003; John and Thomas 2008). Thus, variations in the RH can induce changes in the shape of a microfibril due to the not entirely connected cellulose molecules, as shown in figure 5d, in the marked areas. Crystalline and amorphous regions showed different values for the DMT modulus, which is in agreement with Cabrera et al. (Cabrera et al. 2011).

For the polymer-coated fibres, fluorescence microscopy was applied before the AFM measurements to identify homogenously coated regions of interest on the paper fibre.

Figure 6 shows the AFM images of a polymer coated fibre. As seen in figure 6a, for 2 % RH, and in figure 6b, for the wet condition, there was no significant swelling of the microfibrils of the fibre in the topography images. This is interpreted as the first indicator of a hydrophobic polymer coating. By checking the mechanical properties such as the DMT modulus and adhesion in figure 6d,f for 2 % RH and figure 6e,g for the wet condition, they also revealed no significant changes when increasing the RH. Cross sections of the red framed areas in figure 6a-g are shown in figure 6h and i. This is interpreted as a strong indicator of the hydrophobicity of the polymer coating. Thus, it is concluded that the presence of a homogenous and stable hydrophobic polymer coating can be inferred from AFM measurements. Unmodified fibres exhibit large changes in mechanical properties, such as the DMT modulus and adhesion, as well as the swelling of microfibrils in topographic images. Hydrophobic coated paper fibres show small changes in mechanical properties and almost no swelling in topographical images when the RH was increased.

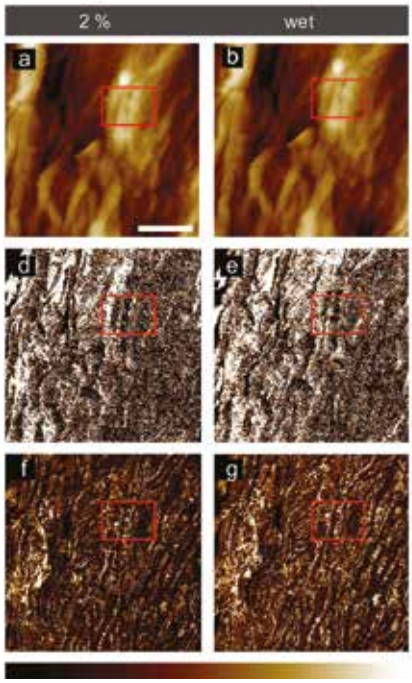

Figure 6:

AFM images of a polymer coated fibre with a homogeneously coated area. a) Topography image at 2 % RH with the corresponding mechanical properties of d) DMT modulus and f) adhesion. b) The topography image under wet conditions with the associated mechanical properties of e) DMT modulus and g) adhesion. The scale bar represents 2 µm. The colour scale ranges from -550 – 550 nm for topography images, from 0 – 300 MPa for DMT modulus maps and from 0 – 10 nN for adhesion maps (Auernhammer et al. 2021a).

CONCLUSION

The atomic force microscopy is a powerful tool to characterise the mechanical properties of single paper fibres. The AFM also allows for the investigation of paper fibres in different environmental conditions, e.g. humid air or water.

It was shown that by the help of force-bending curves obtained with a colloidal probe AFM, it was possible to create a detailed mechanical picture of the paper fibre. Mechanical properties such as adhesion and dissipation, bending ability, contact stress, and strain could be identified. In general, the bending ability increased as RH increased.

The nanomechanical mapping also allowed for further insights into the local mechanics of coated and uncoated fibres. For uncoated fibres, crystalline and amorphous regions could be identified in the topography images, especially in the mechanical property maps. When increasing the RH, the topography images exhibited swollen microfibrils, and the microfibrils changed in size and shape. The swelling and therefore the softening of the fibre apparently started in the non-ordered regions. If the fibres were coated with the hydrophobic polymer, no swelling of the microfibrils could be found in the topography images, and no significant changes in the mechanical properties occurred.

Acknowledgement:

The authors would like to thank the Deutsche Forschungsgemeinschaft under grant PAK 962 project numbers 405549611, 405422877, 405422473 and 52300548 for financial support.

Special thanks to:

Alena K. Bell, Marcus Schulze, Yue Du, Lukas Stühn, Sonja Wendenburg, Isabelle Pause, Markus Biesalski, Wolfgang Ensinger, Anna Lisa Eichhorn, Lars-Oliver Heim, Tom Keil, Binbin Lin, Jan-Lukas Schäfer, and Bai-Xiang Xu

References

Auernhammer J et al. (2021a) Nanomechanical characterisation of a water-repelling terpolymer coating of cellulosic fibres Cellulose doi:10.1007/s10570-020-03675-9

Auernhammer J, Keil T, Lin B, Schäfer J-L, Xu B-X, Biesalski M, Stark RW (2021b) Mapping humidity-dependent mechanical properties of a single cellulose fibre Cellulose doi:10.1007/s10570-021-04058-4

B. Pittenger NE, and C. Su (2012) Quantitative mechanical property mapping at the nanoscale with Peak-Force QNM Application Note 128, Bruker Nano Surfaces Division doi:https://www.bruker.com/fileadmin/user_upload/8-PDF-Docs/SurfaceAnalysis/AFM/ApplicationNotes/Quantitative_Mechanical_Property_Mapping_at_the_Nanoscale_with_PeakForceQNM-AN128-RevB0-AppNote.pdf,

Bump S et al. (2015) Spatial, spectral, radiometric, and temporal analysis of polymer-modified paper substrates using fluorescence microscopy Cellulose 22:73-88 doi:10.1007/s10570-014-0499-5

Cabrera RQ, Meersman F, McMillan PF, Dmitriev V (2011) Nanomechanical and Structural Properties of Native Cellulose Under Compressive Stress Biomacromolecules 12:2178-2183 doi:10.1021/bm200253h

Delaney JL, Hogan CF, Tian JF, Shen W (2011) Electrogenerated Chemiluminescence Detection in Paper-Based Microfluidic Sensors Anal Chem 83:1300-1306 doi:10.1021/ac102392t

Derjaguin BV, Muller VM, Toporov YP (1975a) EFFECT OF CONTACT DEFORMATIONS ON ADHESION OF PARTICLES J Colloid Interface Sci 53:314-326 doi:10.1016/0021-9797(75)90018-1

Derjaguin BV, Muller VM, Toporov YP (1975b) Effect of contact deformations on ahesion of particles Journal of Colloid and Interface Science 53:314-326 doi:10.1016/0021-9797(75)90018-1

Dunlop-Jones N (1996) Wet-strength chemistry Paper Chemistry:98 - 119

Fidale LC, Ruiz N, Heinze T, El Seoud OA (2008) Cellulose swelling by aprotic and protic solvents: What are the similarities and differences? Macromol Chem Phys 209:1240-1254 doi:10.1002/macp.200800021

Gumuskaya E, Usta M, Kirci H (2003) The effects of various pulping conditions on crystalline structure of cellulose in cotton linters Polym Degrad Stabil 81:559-564 doi:10.1016/S0141-3910(03)00157-5

Gurnagul N, Page DH (1989) The difference between dry and rewetted zero-span tensile-strength of paper Tappi J 72:164-167

H. Pahl BE (1988) Use of polyamide resins in board Tappi Wet and Dry Short Course

Hayes RA, Feenstra BJ (2003) Video-speed electronic paper based on electrowetting Nature 425:383-385 doi:10.1038/nature01988

Hertz H (1881) Über die Berührung fester elastischer Körper (on the contact of elastic solids), Journal für die reine und angewandte Mathematik 92:156–171

Janko M et al. (2015) Cross-Linking Cellulosic Fibers with Photoreactive Polymers: Visualization with Confocal Raman and Fluorescence Microscopy Biomacromolecules 16:2179-2187 doi:10.1021/acs.biomac.5b00565

John MJ, Thomas S (2008) Biofibres and biocomposites Carbohyd Polym 71:343-364 doi:10.1016/j.carbpol.2007.05.040

Johnson KL, Kendall K, Roberts AD (1971) SURFACE ENERGY AND CONTACT OF ELASTIC SOLIDS Proceedings of the Royal Society of London Series a-Mathematical and Physical Sciences 324:301-& doi:10.1098/rspa.1971.0141

Liana DD, Raguse B, Gooding JJ, Chow E (2012) Recent Advances in Paper-Based Sensors Sensors 12:11505-11526 doi:10.3390/s120911505

Lindman B, Karlstrom G, Stigsson L (2010) On the mechanism of dissolution of cellulose J Mol Liq 156:76-81 doi:10.1016/j.molliq.2010.04.016

Rogovin ZA, Gal'brajch LS (1983) Die chemische Behandlung und Modifizierung der Zellulose. Stuttgart u.a.

Ruettiger C et al. (2016) Redox-mediated flux control in functional paper Polymer 98:429-436 doi:10.1016/j.polymer.2016.01.065

Yano T, Ohtani H, Tsuge S, Obokata T (1991) DETERMINATION OF WET-STRENGTH RESIN IN PAPER BY PYROLYSIS-GAS CHROMATOGRAPHY Tappi J 74:197-201